Infrared dielectric function and phonon modes of highly disordered $(Al_xGa_{1-x})_{0.52}In_{0.48}P$

T. Hofmann*
Solid State Physics Group, Faculty of Physics and Geosciences, University of Leipzig, 04103 Leipzig, Germany

G. Leibiger and V. Gottschalch
University of Leipzig, Faculty of Chemistry and Mineralogy, Department of Solid State Chemistry, 04103 Leipzig, Germany

Ines Pietzonka
Lund University, Department of Solid State Physics, Box 118, S-22100 Lund, Sweden

M. Schubert
Center for Microelectronic and Optical Materials Research, and Department of Electrical Engineering, University of Nebraska-Lincoln, Nebraska 68588
and Solid State Physics Group, Faculty of Physics and Geosciences, University of Leipzig, 04103 Leipzig, Germany
(Received 16 March 2001; published 28 September 2001)

Dielectric function spectra and phonon modes of highly disordered $(Al_xGa_{1-x})_{0.48}In_{0.52}P$, i.e., solid solutions with nearly randomly distributed cations, lattice matched to GaAs, are studied for Al compositions $x=0$, 0.33, 0.48, 0.7, 0.82, and 1 using far-infrared ellipsometry and Raman scattering. An anharmonic oscillator model approach is employed for line-shape analysis of the $(Al_xGa_{1-x})_{0.48}In_{0.52}P$ dielectric function. A complex phonon mode behavior for the random-alloy solid solutions is found: (i) two (one weak GaP-like and one strong InP-like or one weak InP-like and one strong AlP-like with TO-LO splitting) bands are present in $Ga_{0.52}In_{0.48}P$ and $Al_{0.52}In_{0.48}P$, respectively, (ii) three (one weak GaP-like, one weak AlP-like, and one strong InP-like) bands dominate the quaternary compounds for $x<0.5$, (iii) the GaP-like band is absent for $x>0.5$, and (iv) three additional modes (AM's) with low polarity occur with small composition dependencies at $AM_1 \sim 313\,cm^{-1}$, $AM_2 \sim 351\,cm^{-1}$, and $AM_3 \sim 390-405\,cm^{-1}$, respectively. Results from polarized Raman measurements agree excellently with the mode scheme developed from the ellipsometry study. Modes AM_1 and AM_2 coincide with CuPt-type superlattice-ordering-induced lattice modes, predicted recently for $Ga_{0.52}In_{0.48}P$ from first-principles calculations [V. Ozoliņš and A. Zunger, Phys. Rev. B **57**, R9404 (1998)] and may be used to identify small degrees of ordering in AlGaInP by far-infrared ellipsometry.

DOI: 10.1103/PhysRevB.64.155206 PACS number(s): 72.10.Di, 78.30.Fs, 78.66.Fd, 63.20.−e

I. INTRODUCTION

The III-V alloy system $Al_{x'}Ga_{y'}In_zP$ has been the subject of intense research since the advent of the molecular beam epitaxy[1,2] (MBE) and the metal-organic vapor phase epitaxy[3] (MOVPE) techniques for semiconductor thin-film deposition. During the last two decades, enormous effort led to the development of optoelectronic devices based on $Al_{x'}Ga_{y'}In_zP$ as active material.[4–7] For $z=0.48$ the alloy can be grown lattice matched to GaAs for Al compositions $x=x'/(1-z)=0-1$.[8] Besides chemical effects due to alloying or effects due to lattice-mismatch-induced strain, spontaneous cationic ordering of CuPt type can drastically affect the physical properties of the solid solution, and the degree of ordering η influences,[9] e.g., band-gap energies, electron effective mass parameters, phonon modes, and electrical transport properties.[10] Therefore, knowledge of the composition, strain, and degree of ordering[11] is crucial for correct tailoring of device constituent properties.

For highly disordered compounds ($\eta \sim 0$), the composition dependence of the room-temperature (RT) direct band-gap energy is $E_g(x,\eta\sim 0)\,[\mathrm{eV}] = 1.899 + 0.683x - 0.12x(1-x)$,[12] where the direct-indirect crossover occurs near $x=0.52$,[13] thereby limiting random-alloy $Al_{0.52x}Ga_{0.52(1-x)}In_{0.48}P$ solid solutions for short-wavelength photonic device applications to 2.24 eV. Most studies have so far have concentrated on $Ga_{0.52}In_{0.48}P$. Knowledge concerning the influence of ordering and composition on the physical properties of alloys with $x>1$ or $z\neq 0.48$ is not exhaustive, and further studies are required. Simultaneous assessment of x for $x\neq 0$ and η is a challenge. Electron microscopy techniques reveal the existence of ordering, but quantitative determination of η is difficult.[10] The redshift of the band gap $\Delta E_g(x,\eta)$ can be used to quantify η upon comparing measured $\Delta E_g(x,\eta)$ values with calculated maximum gap reduction values for perfect ordering $(\eta=1)\Delta E_g(x,1)$. Theoretical values for $\Delta E_g(x,1)$ exist only for $z=0.5$ and $x=0,1$ ($Ga_{0.5}In_{0.5}P$: 430 meV, $Al_{0.5}In_{0.5}P$: 270 meV).[14,9] Experimental values $\Delta E_g(x=0.48,\eta=1)$, deduced recently from generalized ellipsometry experiments,[15] agreed well with a linear interpolation between the theoretical results for $Ga_{0.5}In_{0.5}P$ and $Al_{0.5}In_{0.5}P$, suggesting that a linear interpolation scheme for the composition dependence of $\Delta E_g(x,1)$ would allow one to classify η for all compositions upon the measured red shift $\Delta E_g(x,\eta)$. However, strong deviations from theoretical results were found experimentally for $Al_{0.52}In_{0.48}P$,[14,16] and further studies shall elucidate $\Delta E_g(x>0.5,\eta=1)$.

A feasible alternative to access strain, composition, and ordering information is to study the phonon mode spectra of

the solid solutions because chemical (composition), structural (strain), and configuration (ordering) effects influence the short-range force constants as well as the long-range electrostatic fields.[17] FIR-transmission[18] and -reflection[19,20] and Raman scattering[21–33] (RS) spectroscopy were employed to study ordering-induced changes in the phonon spectrum of $Ga_{0.52}In_{0.48}P$, whereas no reports seem to exist for solutions with $x>0$. CuPt ordering induces additional modes in the acoustic region at 60 cm^{-1} and 205 cm^{-1}, which were identified as L-to-Γ folded acoustic phonons.[30,33] A new peak emerges in the optic region with increasing η at $\sim$354 cm^{-1}, which was identified as the LO mode with A_1 symmetry.[18,19,28,29] After early studies on polycrystalline samples using FIR and RS spectroscopy,[34–37] it was thought that $Ga_{1-z}In_zP$ is a one-mode system, supported by results from the modified random isodisplacement model of Chang and Mitra.[38] An additional feature was subject to diverse interpretation.[34–37] Jusserand and Slemkes[39] performed detailed studies of single-crystalline samples and stated a ''modified'' two-mode behavior, where two LO modes—one InP-like and one GaP-like—and one InP-like TO mode occurred for all compositions. In a simple presentation, the frequencies of the Ga (In) impurity modes in bulk InP (GaP) may determine whether the system will display a one- or two-mode behavior. A pure one-mode behavior can only be pictured if both impurity modes merge with their opposite TO modes. Naively, but nonetheless in a strict sense, a ''modified'' two-mode system cannot exist in this presentation, because of the ''alternation'' rule, which requires that each TO mode neighbors its LO mode.[40] The GaP-like TO mode, adjacent to InP-like LO, occurs indeed,[41] but is often subsumed by the strong LO line shape and therefore difficult to retrieve from unpolarized Raman spectra. The GaP-like TO mode was clearly resolved in recent FIR-reflectivity and -transmission studies[18,19] and is also detected in the present study. Recently, Ozoliņš and Zunger reported on vibrational properties of random-alloy and CuPt-type ordered $Ga_{0.5}In_{0.5}P$ from first-principles density-functional linear-response theory calculations.[17,42] For random-alloy $Ga_{0.5}In_{0.5}P$ two strong pairs of LO and TO modes were found, where each mode contains contributions from both cations. These modes agree well with the GaP- and InP-like TO and LO modes found in Raman and FIR experiments. In addition, the calculated partial TO- and LO-decomposed phonon density of states contains several weak side bands with mixed Ga and In contributions, and results obtained in the present paper endorse a complex phonon spectrum beyond the ''two-mode'' picture.

The phonon mode behavior of AlGaInP is still controversial. Some reports conclude a three-mode behavior,[43,44] whereas others assign a ''partially'' three-mode behavior.[45] RS studies on (presumably disordered) $Al_{1-z}In_zP$ ($0.4<z<0.7$) were reported by Bour *et al.*,[46,47] and the authors assigned a two-mode behavior with one InP-like and one AlP-like band. Four groups reported RS data from $(Al_xGa_{1-x})_{0.52}In_{0.48}P$,[43–45,48] where two studies cover the full range of composition x.[43,45] The AlP-like LO mode was found to vary almost linearly with x, whereas small bowing is required to describe the change of the GaP- and InP-like LO modes. The InP-like LO mode was observed for all x. GaP- and AlP-like LO modes were observed in the range $0\leqslant x\leqslant 0.4$ and $0.16\leqslant x\leqslant 1$, respectively.[45] Only Kubo *et al.*[45] and Asahi, Emura, and Gonda[44] reported on a clear observation of InP-like TO modes. No report presented evidence for the existence of GaP- and AlP-like TO modes, nor does any work address the influence of ordering. Lack of accurate knowledge of the $Al_{x'}Ga_{y'}In_zP$ lattice mode behavior requires further experiments. To begin with, the phonon mode behavior of nearly random-alloy solid solutions shall be established in the present work, where three major TO-LO bands are clearly assigned for the quaternary samples studied here.

FIR transmission and reflection experiments constitute an alternative to RS spectroscopy in order to determine lattice modes of III-V compound materials. The link between the FIR data and the materials' lattice modes is the dielectric function ε, which obeys poles and zeros at TO and LO frequencies.[40,49,50] No data of accurate ε values at FIR wavelengths for $Al_{x'}Ga_{y'}In_zP$ quaternary alloys have been reported so far. Reflectivity data of ordered and random-alloy $Ga_{0.52}In_{0.48}P$ were presented by Alsina *et al.*, but simple model assumptions for parametrization of ε resulted in poor agreement between experimental and calculated data only. Precise data for ε were not extracted from the experiments.[18–20]

Data accuracy and sensitivity to thin film properties achievable by spectroscopic ellipsometry (SE) is superior over standard reflection or transmission intensity measurement techniques.[51] SE can be employed at wavelengths, which match the phonon frequencies of III-V alloys.[52] This technique has become available recently as feasible technique for characterization of free-carrier and phonon properties in III-V semiconductor bulk materials and thin epitaxial layers.[53] Fast, convenient, precise, and nondestructive characterization of single layers, superlattices, or complex heterostructures provided phonon and free-carrier information for, e.g., GaAs,[52,54] SiC,[55] GaAsN,[56,57] GaInAsN,[58,59] GaN,[60,61] AlGaN,[62] and AlInN.[63] In this work we will perform a comparative study of the lattice vibration properties of $(Al_xGa_{1-x})_{0.52}In_{0.48}P$ using FIR-SE and RS. $(Al_xGa_{1-x})_{0.52}In_{0.48}P$ is known to exhibit long-range chemical CuPt ordering, regardless of the composition x.[10,16,64] Therefore, the samples chosen here are highly disordered and were studied at visible wavelengths[12] prior to their investigation here. Accurate line-shape analysis of the FIR-SE data is presented. The lattice modes are then obtained through model line-shape functions and compared with those observed in RS data collected in this work, as well as with those presented in the literature previously.

II. THEORY

A. IR dielectric lattice response

Contributions to the dielectric function ε of semiconductors at FIR wavelengths due to resonant excitation of polar lattice vibrations are commonly described using the harmonic oscillator presentation.[40,50,65] Materials with multiple phonon branches, such as alloys, require sets of multiple

oscillators for appropriate description of ε. Phonon coupling induces anharmonic resonance behavior. Anharmonic oscillator functions with Lorentzian-type broadening have been used successfully for accurate modeling of ε obtained from several multiple-phonon-mode materials.[60,66–70] In this work the factorized form of the anharmonic Lorentzian sum presentation is employed for the parametrization of the $(Al_xGa_{1-x})_{0.52}In_{0.48}P$ dielectric function[66,71]

$$\varepsilon^{(L)} = \varepsilon_\infty \prod_{i=1}^{v} \frac{\omega^2 + i\gamma_{\mathrm{LO},i}\omega - \omega_{\mathrm{LO},i}^2}{\omega^2 + i\gamma_{\mathrm{TO},i}\omega - \omega_{\mathrm{TO},i}^2}, \tag{1}$$

where $\omega_{\mathrm{LO},i}$, $\gamma_{\mathrm{LO},i}$, $\omega_{\mathrm{TO},i}$, and $\gamma_{\mathrm{TO},i}$ are the frequency and the broadening values of the ith LO and TO phonons, respectively, and index i runs over v modes. For further information regarding the history and applicability of Eq. (1), the reader is referred to recent publications and discussions given therein.[60,69,70]

B. Low-polarity modes

Convenient treatment of infrared-active modes with small polarity within the anharmonic oscillator approximation was discussed recently.[60,61] Contributions to ε due to m ''additional modes'' (AM's) with small LO-TO splitting values $\delta\omega_k^2 \equiv \omega_{\mathrm{LO},k}^2 - \omega_{\mathrm{TO},k}^2$ can be factorized in ε:

$$\varepsilon^{(L+\mathrm{AM})}(\omega) = \varepsilon^{(L)}(\omega) \prod_{k=1}^{m} \left(1 + \frac{i\delta\gamma_k\omega - \delta\omega_k^2}{\omega^2 + i\gamma_{\mathrm{AM},k}\omega - \omega_{\mathrm{AM},k}^2} \right), \tag{2}$$

with $\omega_{\mathrm{TO},k} \equiv \omega_{\mathrm{AM},k}$, $\gamma_{\mathrm{TO},k} \equiv \gamma_{\mathrm{AM},k}$, and $\delta\gamma_k \equiv \gamma_{\mathrm{LO},k} - \gamma_{\mathrm{TO},k}$. For $\delta\gamma_k \sim 0$ and small values $\mathrm{Im}\{\varepsilon^{(L)}\}$ for $\omega \sim \omega_{\mathrm{AM},k}$, the following conditions can be read from Eq. (2): $\delta\omega_k^2 < 0$ $(\delta\omega_k^2 > 0) \leftrightarrow \omega_{\mathrm{AM},k}$ is a local mode, i.e., $\omega_{\mathrm{TO},i} < \omega_{\mathrm{AM},k} < \omega_{\mathrm{LO},i}$ ($\omega_{\mathrm{AM},k}$ is a gap mode, i.e., $\omega_{\mathrm{LO},i} < \omega_{\mathrm{AM},k} < \omega_{\mathrm{TO},i+1}$).[60]

C. Free-carrier contribution

The AlGaInP epitaxial layers were deposited on Si-doped GaAs substrates. For a correct model description of the FIR response of the samples, the contribution of the free carriers within the substrates must be considered. The classical Drude approximation holds with sufficient accuracy for description of contributions from free carriers to ε of III-V semiconductors. A single-specie[54] free-carrier plasma contributes $\varepsilon^{(\mathrm{FC})}$ to $\varepsilon(\omega)$,[49,50]

$$\varepsilon^{(\mathrm{FC})}(\omega) = -\varepsilon_\infty \frac{\omega_p^2}{\omega(\omega + i\gamma_p)}. \tag{3}$$

The screened plasma frequency ω_p is related to the free-carrier concentration N, ε_∞, and the free-carrier effective mass m^*,

$$\omega_p = \left(\frac{Nq^2}{\varepsilon_\infty \varepsilon_0 m^*} \right)^{1/2}, \tag{4}$$

where ε_0 is the vacuum permittivity and q the carrier charge. In a constant-carrier-scattering-regime, the connection between the plasma broadening parameter γ_p and the optical carrier mobility parameter μ is $\gamma_p = q(m^*\mu)^{-1}$.[65] Plasmons interact with LO phonons, and LO-phonon-plasmon (LPP) coupling has been observed by FIR spectroscopy in n-type GaAs (Ref. 68) and also in p-type GaAs.[54] The LPP-mode frequencies can be diverted from the roots of ε and split for n-type GaAs into low-frequency (LPP^-) and high-frequency branches (LPP^+).[65]

D. SE data analysis

Ellipsometry determines the complex reflectance ratio ρ,

$$\rho \equiv \frac{r_p}{r_s} = \tan\Psi \exp i\Delta, \tag{5}$$

where r_p and r_s are the complex Fresnel reflection coefficients for light polarized parallel (p) and perpendicular (s) to the plane of incidence, respectively.[72] Ψ and Δ denote the standard ellipsometric parameters. Ψ and Δ, measured on layered samples, depend on all materials' dielectric functions and thickness, and the incident wavelength, in general. Model calculations are needed for SE data analysis.[51] Models must invoke appropriate physical relationships, which must render the dielectric response studied. Materials' physical quantities, such as frequencies, amplitudes, and broadening parameters of charged lattice resonances, follow then through modeling the materials' dielectric functions ε.[51] Parameters with significance are varied during data analysis until calculated and measured data match as close as possible (best fit). Least-squares approaches to minimize weighted test functions (maximum likelihood methods), such as the Levenberg-Marquardt algorithm,[73] are employed for fast convergence.

The model used here accounts for the layer sequence substrate/buffer/epilayer, and all materials are treated isotropic. The model dielectric functions (MDF's) in Secs. II A and II B provide ε for the n-type doped GaAs substrate [Eq. (1), $v=1$, and Eq. (3) with $m^* = 0.067 m_e$ for GaAs] and the undoped GaAs buffer [Eq. (1), $v=1$] with $\omega_{\mathrm{TO}} = 267.7\,\mathrm{cm}^{-1}$, $\omega_{\mathrm{LO}} = 291.3\,\mathrm{cm}^{-1}$, $\gamma_{\mathrm{TO}} = \gamma_{\mathrm{LO}} = 5.6\,\mathrm{cm}^{-1}$, and $\varepsilon_\infty = 11.0$, common to both substrate and buffer.[74] N and μ need to be varied, and account for the free-carrier response within the substrate. The thickness of the buffer layer d_{buffer} is also an adjustable parameter.

Two methods for extracting ε of the $(Al_xGa_{1-x})_{0.52}In_{0.48}P$ layers were pursued here.

(A1) Modeling of ε using the MDF [Eqs. (1) and (2) with $v=3$, $m \leqslant 3$] by adjusting all corresponding MDF parameters.

(A2) Performing a wavelength-by-wavelength (point-by-point) fit for ε.

Both approaches result in numerical reduction of the substrate/buffer optical effects from the SE data, and both require the $(Al_xGa_{1-x})_{0.52}In_{0.48}P$ layer thickness d as necessary input parameter. These thickness values were known from a previous analysis of UV-VIS SE data.[12] A1 also provided enough sensitivity to the substrate parameters N and μ, and d_{buffer}. A2 was employed after performing A1, and N, μ, and d_{buffer} were used as input parameters obtained by A1

TABLE I. Sample parameters for the $(Al_xGa_{1-x})_{0.52}In_{0.48}P$ layers studied in this work. All samples were grown at 720 °C by MOVPE on (001) GaAs with 6° miscut toward the nearest (111) Ga plane. Further growth parameters are given in Ref. 12. The free-carrier concentration N and mobility μ of the Si-doped GaAs substrate, the GaAs buffer layer thickness d_{buffer}, and ε_∞ of the $(Al_xGa_{1-x})_{0.52}In_{0.48}P$ layers are best-fit results from the FIR-SE analysis. Error limits (in parentheses) correspond to 90% reliability.

Sample	*A*	*B*	*C*	*D*	*F*	*G*
x	0	0.33	0.48	0.7	0.82	1
d [nm]	801	951	1224	262	413	913
d_{buffer} [nm]	198(6)	159(9)	266(9)	200(13)	154(3)	167(20)
ε_∞	9.1(0.1)	8.7(0.1)	8.6(0.1)	8.4(0.1)	8.3(0.1)	8.1(0.1)
N(300 K) $[10^{17}\,cm^{-3}]$	7.5(0.03)	4.72(0.02)	27.5(0.04)	7.2(0.06)	9.8(0.01)	7.4(0.1)
μ $[10^3\,cm^2/(V\,s)]$	2.28(0.02)	2.25(0.02)	0.68(0.03)	1.58(0.05)	2.0(0.01)	4.2(0.3)
LPP^- $[cm^{-1}]$	219	186	259	216	224	218
LPP^+ $[cm^{-1}]$	334	311	541	331	358	333

prior to A2. Detailed discussions on parameter correlation issues, proper data noise treatment, and ''best-choice-fitting'' procedures in infrared ellipsometry data analysis can be found in Refs. 60, 69, and 70, and references therein, and shall not be reiterated here.

We finally note that the isotropic model will be incorrect if an appreciable degree of orientational order would be present within the $(Al_xGa_{1-x})_{0.52}In_{0.48}P$ layers. In this case a uniaxial model must be employed. This idea, however, is not pursued any further in this work since we start from the assumption of complete cationic orientation disorder, and for the samples studied here, order-induced birefringence effects will be neglected.

III. EXPERIMENT

Epitaxial $(Al_xGa_{1-x})_{0.52}In_{0.48}P$ layers with A1 compositions $x=0$, 0.33, 0.48, 0.7, 0.82, and 1 were grown by metalorganic vapor-phase epitaxy at 720 °C on (001) GaAs with 6° miscut towards the nearest (111) Ga plane (Table I). Prior to the quaternary layers, a GaAs-buffer layer with thickness of ~300 nm was deposited. All epitaxial layers were intentionally undoped. The thicknesses of the AlGaInP alloy layers range from 262 to 1224 nm. (See Table I and Ref. 12.) All samples were analyzed by transmission electron microscopy to confirm their highly disordered state. The selected-area diffraction pattern did not or only minimally revealed additional spots due to the alternating sublattice planes of CuPt-ordered compounds.[75] RT measurements for all samples were performed by SE and RS for wave numbers from 100 to 600 cm^{-1} and with a resolution of 2 cm^{-1}. The FIR-SE measurements were carried out at 50° and 70° angles of incidence using a prototype, rotating analyzer, Fourier-transform-based ellipsometer, which was equipped with a He-cooled bolometer detector system.[53] RS measurements were performed in the scattering geometries $z(y',y')\overline{z}$ and $y'(x',z)\overline{y'}$ to distinguish between LO and TO modes,[76] where x, y, z, x', and y' denote the crystal axes [100], [010], [001], [110], and $[1\bar{1}0]$, respectively. In the $z(y',y')\overline{z}$ $[y'(x',z)\overline{y'}]$ scattering geometry LO [TO] modes are allowed and TO [LO] modes are forbidden, respectively.[65] RS measurements in $z(y',y')\overline{z}$ geometry for samples *A*, *D*, *E*, and *F* were performed using the 5145-Å line of an argon-ion laser as the excitation source. The 4579-Å line of the same excitation source was used for the measurement of samples *B* and *C*. The size of the laser beam was ~2 mm on the sample surface. Raman scattering measurements in $y'(x',z)\overline{y'}$ geometry were performed for all samples using the 4579-Å line of the laser source. The laser source was focused on the sample surface using a ×100 objective, and the laser spot size was ~1 μm.

IV. RESULTS AND DISCUSSION

A. FIR-SE

Figure 1 depicts experimental (dashed line) and calculated (solid line, approach A1) FIR-SE Ψ spectra for sample *B*

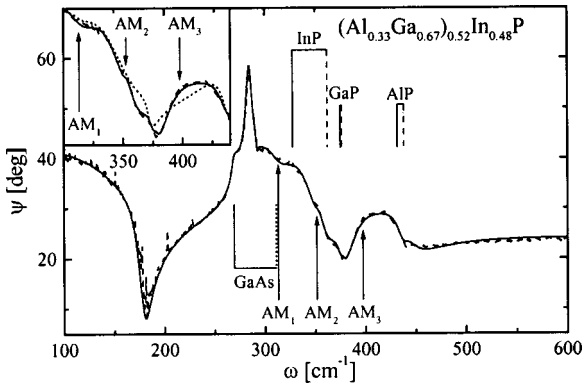

FIG. 1. Experimental (dashed line) and calculated (solid line) FIR-SE Ψ spectra at 50° angle of incidence for sample *B*. InP-, GaP-, and AlP-like TO (solid vertical lines) and LO (dashed vertical lines) modes are indicated by brackets. The reststrahlen band of the *n*-type doped GaAs substrate extends between ω_{TO}(GaAs) (solid vertical line) and LPP^+(GaAs) (dotted vertical line). Low-polarity modes AM_1–AM_3 were added to model ε of the AlGaInP layer adequately. The inset enlarges the spectral region of AM_1–AM_3. The dotted line presents the best-fit line shape without AM_1–AM_3.

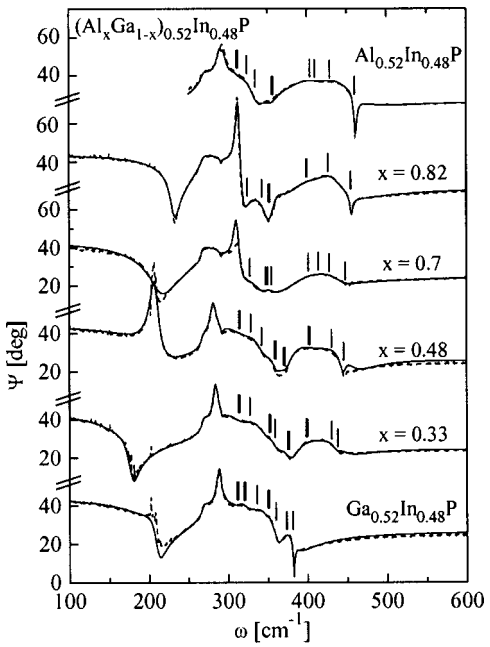

FIG. 2. Experimental (dashed lines) and calculated (solid lines) FIR-SE Ψ spectra of $(Al_xGa_{1-x})_{0.52}In_{0.48}P$/GaAs at 50° angle of incidence. Vertical lines indicate all TO, LO, and AM modes included into the MDF for ε of each AlGaInP layer. The GaAs TO-LPP$^+$ bands reflect the different doping and carrier mobility levels within the Si-doped substrates (Table I).

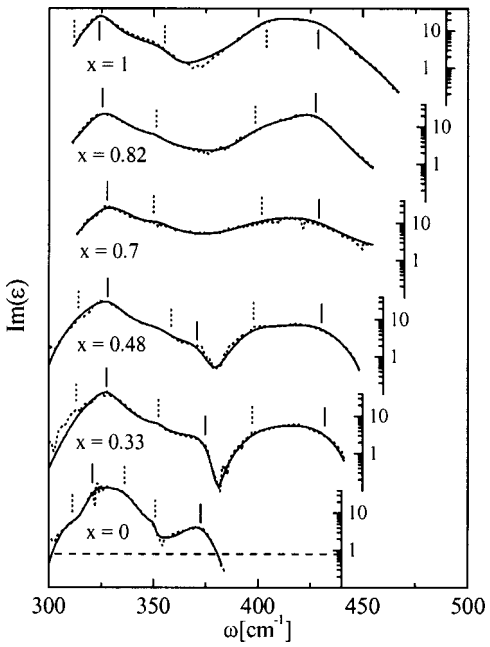

FIG. 3. Point-by-point inverted (dotted lines) and MDF (solid lines) Im(ε) spectra. Vertical lines indicate TO (solid line) and AM- (dotted line) mode parameters within the MDF, which coincide with spectrally local maxima of Im(ε). The dashed line represents the experimental uncertainty in Ψ, which limits determination of small Im(ε) values (shown only for sample *A* with $x=0$).

with $x=0.33$. Presentation of Δ spectra is omitted throughout this work for brevity. The reststrahlen band of the *n*-type GaAs substrate extends between ω_{TO} (267 cm^{-1}, solid vertical line) and LPP$^+$(311 cm^{-1}, dotted vertical line; see also Table I), and dominates the polarized reflectivity at the long-wavelength end of Fig. 1. The strong loss of *p*- (minimum in Ψ) and *s*-polarized reflectivity (maximum in Ψ) at $\omega \sim 180\,\mathrm{cm}^{-1}$ and $\omega \sim 284\,\mathrm{cm}^{-1}$, respectively, is attributed to plasmon-phonon-mode-induced surface-bound electromagnetic wave propagation effects with pseudopolariton character at the substrate/buffer interface. (See Sec. 2.2 in Ref. 56, and references therein.) Above $\sim$311 cm^{-1} the AlGaInP layer causes fine structure in the FIR spectrum of Ψ. (Refer, e.g., to the flat Ψ spectra of nitrogen-rich GaAs layers given in Fig. 7 of Ref. 58.) The fine structure above the GaAs-substrate-LPP$^+$ mode contains multiple bands with anharmonic character. We have identified the strongest contributions as InP-, GaP-, and AlP-like TO (solid vertical lines) and LO (dashed vertical lines) modes, which are indicated by brackets in Fig. 1. These modes bound the InP-, GaP-, and AlP-like reststrahlen bands of the quaternary alloy. Their frequencies were obtained from comparative analysis of the FIR-SE spectra and RS spectra, which will be discussed further below. The three binary constituents of the $(Al_{0.33}Ga_{0.67})_{0.52}In_{0.48}P$ layer produce the major contributions to ε and impose subtle modifications on Ψ above the high-frequency edge of the GaAs reststrahlen band. We included three anharmonic oscillator terms within the MDF to account for the InP-, GaP-, and AlP-like bands and to obtain their TO and LO phonon frequency parameters. Three low-polarity modes AM_1-AM_3 were further added to model ε of the $(Al_{0.33}Ga_{0.67})_{0.52}In_{0.48}P$ layer adequately. Although of small amplitude, these modes are required for accurate reproduction of the experimental line shape. The inset in Fig. 1 enlarges the region where modes AM_1-AM_3 occur, and the

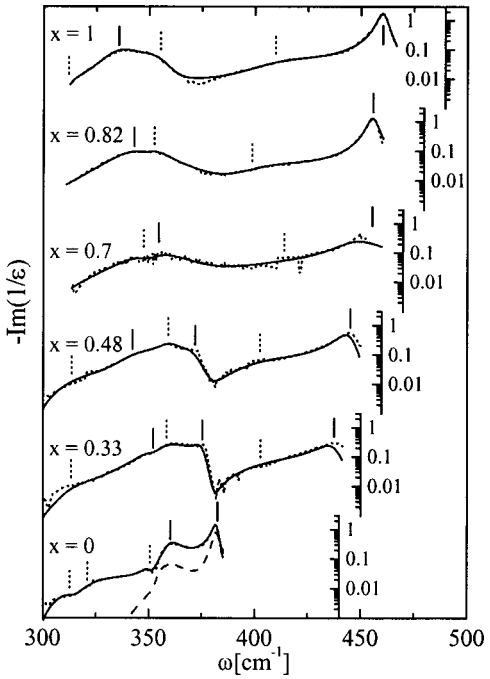

FIG. 4. Same as Fig. 3 for Im($-1/\varepsilon$). Note that the experimental uncertainty in Ψ propagates nonlinearly into sensitivity limits for small Im($-1/\varepsilon$) values (dashed line shown only for sample *A* with $x=0$).

TABLE II. Best-fit results for TO frequencies and broadening parameters from FIR-SE analysis (all values in cm^{-1}). Error limits (in parentheses) correspond to 90% reliability.

Sample	*A*	*B*	*C*	*D*	*F*	*G*
ω_{TO}^{AM1}	311.2(0.3)	313.0(15.2)	313.5(1.7)			311.8(1.1)
γ_{TO}^{AM1}	16.5(2.7)	19.6(3.4)	30.0(3.0)			13.1(6.0)
ω_{TO}^{InP}	320.5(0.5)	327.2(0.2)	328.4(0.8)	327.6(1.1)	325.5(0.2)	324.3(0.2)
γ_{TO}^{InP}	14.1(1.4)	15.3(0.6)	17.1(1.2)	22.3(2.4)	18.6(0.3)	12.7(0.6)
ω_{TO}^{*}	336.2(0.4)					
γ_{TO}^{*}	19.8(0.9)					
ω_{TO}^{AM2}	350.6(0.4)	352.4(0.8)	358.4(2.4)	350.8(2.6)	351.2(1.0)	355.8(1.7)
γ_{TO}^{AM2}	3.7(0.8)	8.1(1.7)	22.1(11.7)	13.3(5.1)	10.3(1.7)	22.7(11.6)
ω_{TO}^{GaP}	372.5(0.3)	374.9(1.2)	370.8(3.1)			
γ_{TO}^{GaP}	17.0(0.6)	13.7(2.4)	28.0(15.1)			
ω_{TO}^{AM3}		397.4(2.2)	398.0(3.7)	401.6(6.3)	398.6(1.3)	403.7(0.7)
γ_{TO}^{AM3}		36.0(4.4)	30.2(8.7)	55.2(16.8)	33.7(2.8)	27.8(1.5)
ω_{TO}^{AlP}		431.8(0.9)	430.1(1.2)	429.0(4.2)	427.4(0.4)	428.9(0.5)
γ_{TO}^{AlP}		34.3(2.1)	37.2(2.6)	39.5(9.6)	23.6(0.8)	31.3(1.0)

dotted line presents the best-fit Ψ spectrum when the low-polarity modes were excluded from the model calculation. All three modes obey small polarity and induce subtle effects on the line shape of ε. Note that all modes obey the ''alternation rule,'' i.e., TO and LO frequencies of multiple phonon mode materials must alternate mutually.[40] Because of $\omega_{TO}^{InP} < \omega^{AM2} < \omega_{LO}^{InP}$, AM_2 is located within the InP-like band, and $\delta\omega^{AM2} = -0.4\,cm^{-1} < 0$ for $x = 0.33$.[60]

Figure 2 shows experimental (dashed lines) and calculated (solid lines, approach A1) FIR-SE Ψ spectra for all samples. Vertical lines indicate the spectral positions of all phonon modes used within the MDF for ε of the AlGaInP layers. The GaAs restrahlen behavior is different for each sample because substrates out of various charges with slightly different doping levels were used for sample deposition (Table I). Figures 3 and 4 present $\mathrm{Im}(\varepsilon)$ and $\mathrm{Im}(-1/\varepsilon)$, respectively, obtained by approaches A1 (solid lines) and A2 (dotted lines). Tables I, II, and III summarize all parameters from the best-fit calculation using A1. It is worth emphasizing the excellent agreement between the point-by-point inverted ε spectra and the MDF model line shape. MDF approaches can subsume small resonance lines into adjacent model lineshapes of larger amplitudes. Subtle features may thereby become wiped out within the resulting spectra, when presented as the ''original'' data. The differences between the point-by-point fit and the MDF spectra in Figs. 3 and 4 are minor only and represent data noise. The dashed lines in Figs. 3 and 4 estimate the sensitivity limit to small absorption values considering the experimental limits for small Δ values, propagated into ε. We have estimated, based on our equipment's present average uncertainty of $\delta\Delta \sim \pm 0.5°$, that values of $\mathrm{Im}(\varepsilon) < 0.7$ cannot be sensed by

TABLE III. Best-fit results for LO frequencies and broadening parameters from FIR-SE analysis (all values in cm^{-1}). Error limits (in parentheses) correspond to 90% reliability. Note that $\omega_{LO}^{AM,k} = \omega_{TO}^{AM,k} + \delta^{AM,k}$ is used.

Sample	*A*	*B*	*C*	*D*	*F*	*G*
$\delta\omega^{AM1}$	1.7(0.1)	0[a]	0[a]			0[a]
$\delta\gamma^{AM1}$	−2.3(0.6)	3.3(0.8)	14.1(2.3)			2.5(1.4)
ω_{LO}^{*}	321.5(1.6)					
γ_{LO}^{*}	37.1(2.6)					
$\delta\omega^{AM2}$	0[a]	−0.4(0.01)	−16.2(0.2)	−2.5(0.4)	1.1(0.1)	0[a]
$\delta\gamma^{AM2}$	1.0(0.3)	2.7(0.9)	5.0(2.8)	6.9(4.6)	0[a]	−6.2(3.4)
ω_{LO}^{GaP}	382.0(0.1)	375.3(1.9)	371.9(5.8)			
γ_{LO}^{GaP}	3.4(0.1)	6.6(1.1)	14.3(3.9)			
ω_{LO}^{InP}	360.1(0.2)	358.4(1.3)	359.9(1.3)	354.5(6.4)	342.9(0.6)	335.0(0.6)
γ_{LO}^{InP}	9.5(0.4)	21.2(2.4)	11.9(3.2)	26.9(11.8)	27.6(1.0)	21.0(0.9)
$\delta\omega^{AM3}$		0[a]	4.8(0.1)	12.1(0.4)	0[a]	6.1(0.1)
$\delta\gamma^{AM3}$		22.6(4.2)	9.1(3.7)	44.8(24.5)	15.6(0.1)	18.8(0.2)
ω_{LO}^{AlP}		437.5(0.4)	444.9(0.3)	448.0(1.7)	455.6(0.1)	460.3(0.1)
γ_{LO}^{AlP}		13.1(0.7)	10.5(0.6)	25.4(3.3)	5.7(0.2)	5.1(0.1)

[a]No sensitivity to parameter; $\delta\omega$ set to 0.

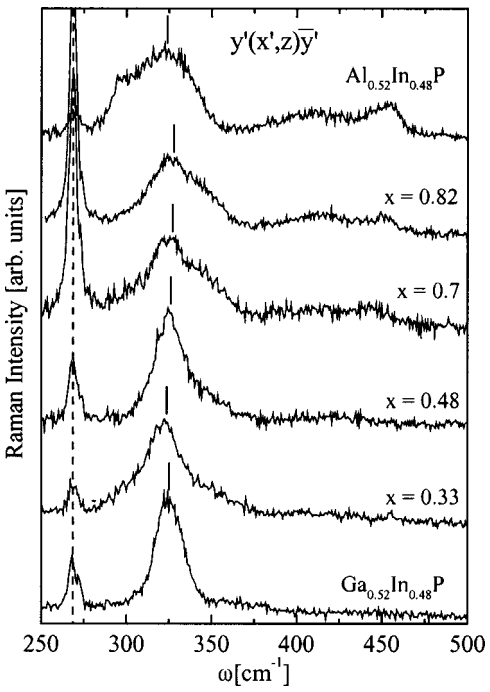

FIG. 5. Raman spectra in $y'(x',z)\bar{y}'$ backscattering geometry (TO allowed, LO forbidden). The GaAs TO mode (vertical dashed line) originates from the substrate and buffer layer. The InP-like TO modes are indicated by vertical lines. The AIP-like TO mode occurs for $x \geqslant 0.7$ at $\omega \sim 400\ \mathrm{cm}^{-1}$, but is too weak for accurate line-shape analysis.

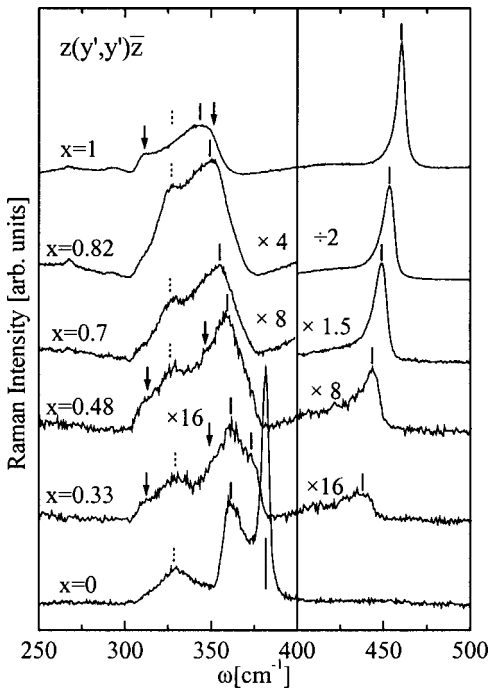

FIG. 6. Raman spectra in $z(y',y')\bar{z}$ backscattering geometry (LO allowed, TO forbidden). LO modes are indicated by vertical solid lines. The InP-like LO mode is strongly excited in all samples and occurs in the range $\sim 340\ \mathrm{cm}^{-1}$ ($x=1$) to $\sim 361\ \mathrm{cm}^{-1}$ ($x=0$). For $x \geqslant 0.33$ the AlP-like LO mode occurs above $\sim 430\ \mathrm{cm}^{-1}$. The InP-like TO mode (dotted vertical lines) is symmetry forbidden, but occurs for all x. For $x=0.33$, 0.48, and 1 modes at $\omega \sim 313\ \mathrm{cm}^{-1}$ and $\omega \sim 351\ \mathrm{cm}^{-1}$ are identical with AM_1 and AM_2 (arrows), which were found in the FIR-SE analysis.

the ellipsometric approach. Note that these uncertainties translate nonlinearly into noise limits for $\mathrm{Im}(-1/\varepsilon)$. (The dashed line in Fig. 4, sample *A*, is shown for example.) It follows directly from Eqs. (1) and (2) that $\mathrm{Im}(\varepsilon)$ and $\mathrm{Im}(-1/\varepsilon)$ peak locally near TO and LO frequencies, respectively. Figure 3 (4) contains vertical lines depicting TO (LO) frequencies as solid lines and AM-mode frequency parameters as dotted lines, representing values given in Tables II and III. As can be seen in Figs. 3 and 4, the MDF TO and LO parameters indeed point to local maximum in spectra $\mathrm{Im}(\varepsilon)$ and $\mathrm{Im}(-1/\varepsilon)$, respectively. For AM modes with small TO-LO splitting, corresponding maxima occur at almost the same frequency in $\mathrm{Im}(\varepsilon)$ and $\mathrm{Im}(-1/\varepsilon)$.

B. Raman spectroscopy

The spectra in Fig. 5 summarize RS studies in $y'(x',z)\bar{y}'$ backscattering geometry (TO allowed, LO forbidden). The vertical dashed line depicts the GaAs TO mode, which originates from the substrate and buffer layer. Short vertical lines indicate the spectral positions of the InP-like TO modes. Their peak positions where determined using Lorenztian line-shape fits.[48] The AlP-like TO mode occurs for $x \geqslant 0.7$ at $\omega \sim 400\ \mathrm{cm}^{-1}$, but was found too broadened for accurate line-shape analysis. The spectrum of the $Al_{0.52}In_{0.48}P$ sample further contains the symmetry-forbidden LO mode of the GaAs buffer layer ($\omega \sim 292\ \mathrm{cm}^{-1}$) and the AlP-like LO mode ($\omega \sim 460\ \mathrm{cm}^{-1}$).

Figure 6 presents Raman spectra obtained in $z(y',y')\bar{z}$ backscattering geometry (LO allowed, TO forbidden). Identified LO modes are indicated by vertical solid lines. The InP-like LO mode is strongly excited in all samples and occurs in the range $\sim 340\ \mathrm{cm}^{-1}$ ($x=1$) to $\sim 361\ \mathrm{cm}^{-1}$ ($x=0$). For $x \leqslant 0.33$ the AlP-like LO mode occurs above $\sim 430\ \mathrm{cm}^{-1}$. The GaP-like LO mode is clearly distinguishable for samples with $x=0$ and $x=0.33$. The InP-like TO mode (dotted vertical lines) is symmetry forbidden, but occurs for all x. For $x=0.33$, 0.48, and 1, additional modes occur at $\omega \sim 313\ \mathrm{cm}^{-1}$ and $\omega \sim 350\ \mathrm{cm}^{-1}$ (vertical arrows), which exactly match the spectral locations of AM_1 and AM_2, assigned already in the FIR-SE analysis. (See also Tables II and III, and note that $\omega_{\mathrm{LO}}^{\mathrm{AM},k} = \omega_{\mathrm{TO}}^{\mathrm{AM},k} + \delta^{\mathrm{AM},k}$.)

C. Lattice modes in AlGaInP

Figure 7 summarizes all TO-, LO-, and AM-mode frequencies obtained from the FIR-SE and RS data. Modes identified from RS spectra are in remarkably good agreement with those derived from our ellipsometry analysis. A complex phonon mode behavior is observed for the nearly random-alloy solid solutions

(i) Two bands are present in $Ga_{0.52}In_{0.48}P$ and $Al_{0.52}In_{0.48}P$, one strong InP- and one weak GaP-like and one weak InP- and one strong AlP-like, respectively.

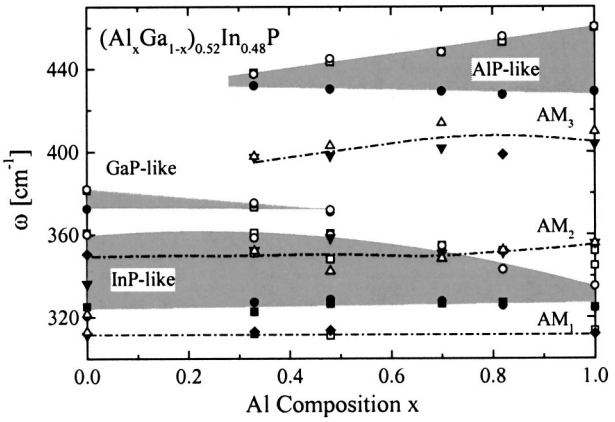

FIG. 7. TO-, LO-, and AM-mode frequency dependences on the Al composition x found in this work (solid symbols: TO; open symbols: LO). Rectangles denote phonon frequencies obtained from Raman spectra. Circles indicate parameter values from FIR-SE analysis. The InP-, GaP-, and AlP-like bands are emphasized by hatched areas. Triangles (TO, up; LO, down) indicate modes AM_1–AM_3, which are shown as diamonds for $\delta\omega_k \sim 0$.

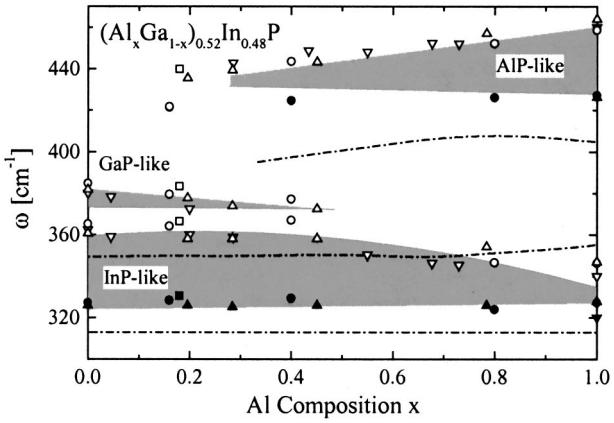

FIG. 8. TO (solid symbols) and LO (open symbols) mode frequencies for $(Al_xGa_{1-x})_{0.52}In_{0.48}P$ reported by Kondow, Minagawa, and Satoh (down rectangles), Kubo *et al.* (circles), Asahi *et al.* (up triangles), and Feng *et al.* (squares). Hatched areas and dash-dotted lines are the same as in Fig. 7.

(ii) Three bands, one weak GaP-like, one weak AlP-like, and one strong InP-like, dominate the quaternary compounds for $x<0.5$.

(iii) The GaP-like band is absent for $x>0.5$.

(iv) Three low-polarity modes with small dispersion occur at $\sim$313 cm^{-1}, $\sim$351 cm^{-1}, and $\sim$400 cm^{-1}, where the first two apparently involve In and/or P, and the last is related to the existence of Al.

The GaP- and AlP-like mode frequencies change linearly with composition x. The InP-like LO mode exhibits small bowing. The frequency dependences are approximately given by

$$\omega_{\mathrm{LO}}^{\mathrm{AlP}}(x) \approx 33.0\ \mathrm{cm}^{-1}x + 427.2\ \mathrm{cm}^{-1},$$

$$\omega_{\mathrm{TO}}^{\mathrm{AlP}}(x) \approx -5.0\ \mathrm{cm}^{-1}x + 432.8\ \mathrm{cm}^{-1} \quad (0.33 \leqslant x \leqslant 1),$$

$$\omega_{\mathrm{LO}}^{\mathrm{InP}}(x) \approx -44.0\ \mathrm{cm}^{-1}x + 19.3\ \mathrm{cm}^{-1}x + 359.5\ \mathrm{cm}^{-1},$$

$$\omega_{\mathrm{TO}}^{\mathrm{InP}}(x) \approx 3.0\ \mathrm{cm}^{-1}x + 323.9\ \mathrm{cm}^{-1} \quad (0 \leqslant x \leqslant 1), \qquad (6)$$

and

$$\omega_{\mathrm{LO}}^{\mathrm{GaP}}(x) \approx -20.9\ \mathrm{cm}^{-1}x + 382.1\ \mathrm{cm}^{-1},$$

$$\omega_{\mathrm{TO}}^{\mathrm{GaP}}(x) \approx -1.7\ \mathrm{cm}^{-1}x + 373.2\ \mathrm{cm}^{-1} \quad (0 \leqslant x \leqslant 0.48). \qquad (7)$$

The dependences for InP-like TO and InP-, GaP-, and AlP-like LO agree well with those given in Ref. 44, except that no second-order term was found here for AlP-like LO. The x dependence of modes AM_1-AM_3 is also given in Fig. 7. The location of AM_1 at $\omega_{AM1} \sim 313\,\mathrm{cm}^{-1}$ is that of a gap mode,[40] and AM_1 occurs below InP-like TO Mode AM_2 at $\omega_{AM2} \sim 351\,\mathrm{cm}^{-1}$ is a local mode within the InP-like band, and mode AM_3 at $\omega_{AM3} \sim 395-405\,\mathrm{cm}^{-1}$ is another gap mode between the GaP- and AlP-like bands.

The broadening parameters in Tables II and III for the GaP-, InP-, and AlP-like modes are substantially larger than those for the pure binary compounds.[77,78] It was already observed that lattice mode broadening parameters of ternary alloys are larger than those for the pure binary constituents.[79,80] Here, the broadening of the GaP-like band increases as x increases from 0 to 0.48. The broadening parameter of the AlP-like TO mode reveals a maximum at approximately $x=0.6$, whereas the LO-mode broadening decreases as x increases from 0.33 to 1. The InP-like band exhibits a maximum broadening at approximately $x=0.6$ for both LO and TO modes. The broadening parameters for the additional modes AM_1-AM_3 are found to remain nearly constant for all compositions studied here.

Modes AM_1 and AM_2 display no or only little dependence on the Al concentration. These modes seem to occur regardless of x. Therefore, eigenvectors of AM_1 and AM_2 should involve In and P displacements. The character of AM_2 changes at $x \sim 0.8$ from a local mode to that of a gap mode. The splitting parameters $\delta\omega^{AM1}$ and $\delta\omega^{AM2}$ are small, except for $x=0.48$. Mode AM_3 occurs only for $x>0$, suggesting involvement of Al. The splitting parameter $\delta\omega^{AM3}$ is small except for $x=0.7$. A peculiarity is seen for $Ga_{0.48}In_{0.52}P$ through the observation of another local mode pair ($\omega_{TO}^{*}=336.2\ \mathrm{cm}^{-1}$, $\omega_{LO}^{*}=321.5\,\mathrm{cm}^{-1}$), located within the InP-like band and which was not observed in samples with $x>0$.

The positions of the InP-, GaP-, and AlP-like bands in the quaternary alloy were partially viewed in the literature, and data reported by different authors are fairly consistent. Figure 8 reviews TO- and LO-mode frequencies obtained from RS investigations reported by Kondow, Minagawa, and Satoh[43] ($0 \leqslant x \leqslant 1$, down rectangles), Kubo *et al.*[45] ($0 \leqslant x \leqslant 1$, circles), Asahi *et al.*[44] ($0 \leqslant x \leqslant 1$, up-triangles), and Feng *et al.*[48] ($x=0.18$, squares) in comparison with results obtained in this work (indicated by hatched areas and dash-dotted lines). Values for InP-like TO and AlP-like LO are

almost consistent. Considerable scatter exists within GaP-like LO data, which is not surprising because this band is very small and likely subsumed by the strong InP-like LO band in RS data. Apparently, no line-shape analysis was performed in Refs. 43, 44, and 45. The only AlP-like TO values, reported by Kubo *et al.*,[45] deviate substantially with decreasing Al content from our ellipsometry results. The assignment for the AlP-like TO mode from spectra shown in Ref. 45 is unclear, and values shown in Ref. 45 are uncertain. No other group observed AlP-like TO in RS spectra, and no such mode is detected in our $z(y',y')\bar{z}$ RS studies. Data for $x=0.18$ reported by Feng *et al.* fit excellently into the scheme developed here, if all values would be shifted up by ~ 4 cm^{-1}. Data for GaP-like TO and AlP-like TO were not reported. No data from FIR reflection or transmission measurements for $x>0$ are available. No group has reported on the occurrence of modes AM_1-AM_3 observed in the present work. The InP-like LO assignment by Kondow, Minagawa, and Satoh[43] in the crossover region between the local- and gap-mode behavior of AM_2 may reflect the unnoticed influence of AM_2 on their RS spectra. Neither of the gap modes AM_1 and AM_3 has been assigned in any work.

AM_1 occurs in $z(y',y')\bar{z}$ Raman spectra for $x=0.33$, 0.48, and 1. For samples with $x=0$, 0.72, and 0.8 this mode is weak and subsumed by the strong InP-like LO mode. Mintairov and Melehin[31] found a very weak ordering-induced mode at 315 cm^{-1} in CuPt-ordered $Ga_{0.52}In_{0.48}P$ Hassine *et al.* reported $z(y',y')\bar{z}$ Raman spectra of ordered $Ga_{0.52}In_{0.48}P$, and although unnoticed by the authors, a weak side band also occurs at $\omega \sim 315$ cm^{-1} (Fig. 3 of Ref. 30). This band can further be recognized within Raman data of ordered $Ga_{0.52}In_{0.48}P$ reported by Mestres *et al.* [Figs. 2(a) and 3(a) in Ref. 29] and Cheong *et al.* (Fig. 1 in Ref. 32).

Mode AM_2 coincides with the mode at 354 cm^{-1}, which was found in CuPt-ordered $Ga_{0.52}In_{0.48}P$.[18,20,28,32,33] AM_2 is seen in our $z(y',y')\bar{z}$ Raman data for samples *B*, *C*, and *F*, and AM_2 occurs in the FIR-SE data for all *x*. Apparently, this mode is inherent to this alloy, similar to AM_1.

Very recently, Ozoliņš and Zunger calculated phonon spectra of perfectly CuPt-ordered $Ga_{0.5}In_{0.5}P$ using first-principles density-functional linear-response theory.[17,42] In essence, the GaP- and InP-like bands are predicted to split into two bands with modes polarized parallel (A_1) or perpendicular (E) to the ordering direction, in accordance with the C_{3v} crystal symmetry of CuPt-ordered $GaInP_2$. The mechanism of how this splitting will emerge for partial ordering is yet unknown, although Ozoliņš and Zunger suggested application of the "η^2 rule," where strength and spectral position should scale with η^2 times the difference of the respective quantity (strength, position) imposed upon perfect order or disorder.[42] Modes AM_1 and AM_2 seem to match the dispersionless E(TO) mode, predicted at 316 cm^{-1}, and the "new" (CuPt-order-induced) mode of A_1 symmetry at ~ 350 cm^{-1}. Because no quantitative method is available yet for determination of small values η for quaternary alloys, we cannot rule out existence of slight CuPt ordering for our samples. We expect residual ordering in all quaternaries, although no or only little superlattice diffraction spots were observed in selected area diffraction pattern. Sample *A* should not contain any ordered domains according to its band gap value ($E_g=1.899$ eV at 300 K).[12] Sample *G* did reveal no diffraction spots, and its growth condition was that of sample 13 in Ref. 16, which was highly disordered. Because AM_1 occurs regardless of *x*, P and/or In should be involved in this mode. The E(TO) mode predicted for $x=0$, $\eta=1$ at 316 cm^{-1} is indeed GaP-like[42] and may also exist for $x>0$ and for very small η values. For our $Ga_{0.52}In_{0.48}P$ sample, AM_1 can be detected by FIR studies, but is not seen in the Raman spectrum. This observation suggests that AM_1 may be very sensitive to small degrees of ordering. CuPt ordering seems to activate modes AM_1 and AM_2 for Raman scattering. According to this line of discussion, samples *A*, *B*, *C*, and *F* should obey some small degrees of ordering, wherein sample *A* is most disordered. In summary, the origin of modes AM_1 and AM_2 is likely ordering. The occurrence of both modes indicates residual ordering in our samples. These modes may be used to monitor small degrees of ordering. Finally, the "η^2 rule" may not apply for spectral positions of superlattice-ordering-induced lattice modes.

The origin of AM_3 remains unclear. AM_3 was not observed for $x=0$, which suggests that this mode could be related to the existence of Al. Because we are not aware of any work, experimental or theoretical, which studies lattice vibration properties of ordered $Al_{0.52}In_{0.48}P$, no assignment can be made for AM_3 at this point. Also, no observation of AM_3 for quaternary alloys was reported. This is not surprising, because AM_3 was also not seen in our RS spectra. To best of our knowledge, no result from FIR experiments was presented for alloys with $x>0$.

V. SUMMARY

An accurate study of the lattice vibration modes in highly disordered $(Al_xGa_{1-x})_{0.52}In_{0.48}P$ over the full range of composition *x* is performed using ellipsometry and Raman techniques comparatively. All AlP-, GaP-, and InP-like TO and LO modes are deduced from FIR-SE data analysis. The lattice modes follow from line-shape analysis of the fir function ε. RS spectra are analyzed using Lorentzian line-shape fits. Raman results are highly consistent with the mode scheme developed from the ellipsometry study. Three additional modes with low polarity are identified upon the FIR-SE analysis. The first two modes, located near ~ 313 and ~ 351 cm^{-1}, are also Raman active and coincide with CuPt-ordering-induced modes, predicted and observed previously for ordered $Ga_{0.52}In_{0.48}P$. The origin of the third mode remains unclear. It is suggested that the first two modes involve In and/or P contributions, whereas the last one is related to the occurrence of Al. All three modes seem to be inherent to this quaternary alloy system, and may become infrared and Raman active upon ordering.

ACKNOWLEDGMENTS

The authors thank V. Ozoliņš and Professor A. Zunger for communicating Ref. 42 prior to publication and for stimulat-

-ing comments. We gratefully acknowledge U. Teschner for technical assistance. We further appreciate helpful discussions with G. Lippold, A. Eifler, and V. Riede. We thank Professor Grill (UL), Professor Woollam (UNL), and B. Rheinländer for continuing interest in our work. Financial support for this study was provided in part by CMOMR at UNL, NSF Contract No. DMI-9901510 and DFG Contract No. Rh28/3-2.

*Corresponding author. Electronic address: Tino.Hofmann @physik.uni-leipzig.de

[1] H. Asahi, Y. Kawamura, H. Nagai, and T. Ikegami, Inst. Phys. Conf. Ser. **63**, 575 (1981).

[2] H. Asahi, Y. Kawamura, and H. Nagai, J. Appl. Phys. **53**, 4928 (1982).

[3] T. Suzuki, I. Hino, A. Gomyo, and K. Nishida, Jpn. J. Appl. Phys., Part 2 **21**, L731 (1982).

[4] Y. Kawamura, H. Asahi, H. Nagai, and T. Ikegami, Electron. Lett. **19**, 163 (1983).

[5] H. Asahi, Y. Kawamura, and H. Nagai, J. Appl. Phys. **54**, 6958 (1983).

[6] D. P. Bour, in *Quantum Well Laser*, edited by P. S. Zory, Jr. (Academic, Boston, 1993).

[7] G. B. Stringfellow, MRS Bull. **22**, 27 (1997).

[8] *Numerical Data and Functional Relationships in Science and Technology*, edited by K.-H. Hellwege and A. M. Hellwege, Landolt-Börnstein, New Series, Group III, Vol. 17 (Springer, Berlin, 1982).

[9] The parameter η is commonly treated as the composition difference of subsequent cationic (or anionic) sublattice planes of the ordered supercell structure, such as in Ref. 10. For $0<x<1$ in $Al_{x(1-z)}Ga_{(1-x)(1-z)}In_zP$ it is thought that Al and Ga locate in common (111) planes and separate from In; i.e., η is treated as the difference of In concentration in subsequent (111) cation planes. Perfect ordering is then possible for $z=0.5$ only. For random alloys with $z\neq 0.5$, such as those lattice matched to GaAs, η can only vary between $0\leqslant \eta/2 \leqslant \min\{z,1-z\}$. Usually, one neglects the remaining $0.02(Ga_xAl_{1-x})$ when comparing experimental data from unstrained solid solutions on (001) GaAs with predicted values for perfect ordered alloys with $z=0.5$. One may consider the remaining $0.02(Ga_xAl_{1-x})$ as being randomly located at group-III sites.

[10] A. Zunger, MRS Bull. **22**, 20 (1997) and references therein.

[11] Biaxial strain associated with deviation from $z=0.48$ because of lattice-mismatch-induced film strain for pseudomorphic growth conditions affects physical properties of the solid solutions. It has been shown for $Ga_{0.5}In_{0.5}P$ that both strain and ordering can lead to band-gap reduction: S.-H. Wei and A. Zunger, Phys. Rev. B **49**, 14 337 (1994).

[12] M. Schubert, J. A. Woollam, G. Leibiger, B. Rheinländer, I. Pietzonka, T. Saß, and V. Gottschalch, J. Appl. Phys. **86**, 2025 (1999).

[13] J. S. Nelson, E. D. Jones, S. M. Myers, D. M. Follstaedt, H. P. Hjalmarson, J. E. Schirber, R. P. Schneider, J. E. Fouquet, V. M. Robbins, and K. W. Carey, Phys. Rev. B **53**, 15 893 (1996).

[14] S.-H. Wei and A. Zunger, Phys. Rev. B **57**, 8983 (1998).

[15] M. Schubert, T. Hofmann, B. Rheinländer, I. Pietzonka, T. Saß, V. Gottschalch, and J. A. Woollam, Phys. Rev. B **60**, 16 618 (1999).

[16] M. Schubert, B. Rheinländer, E. Franke, I. Pietzonka, J. Skriniarova, and V. Gottschalch, Phys. Rev. B **54**, 17 616 (1996).

[17] V. Ozoliņš and A. Zunger, Phys. Rev. B **57**, R9404 (1998).

[18] F. Alsina, J. D. Webb, A. Mascarenhas, J. F. Geisz, J. M. Olson, and A. Duda, Phys. Rev. B **60**, 1484 (1999).

[19] F. Alsina, H. M. Cheong, J. D. Webb, A. Mascarenhas, J. F. Geisz, and J. M. Olson, Phys. Rev. B **56**, 13 126 (1997).

[20] F. Alsina, N. Mestres, A. Nakhli, and J. Pascual, Phys. Status Solidi B **215**, 121 (1999).

[21] M. Kondow and S. Minagawa, J. Appl. Phys. **64**, 793 (1988).

[22] M. Kondow, H. Kakibayashi, S. Minagawa, Y. Inoue, T. Nishino, and Y. Hamakawa, Appl. Phys. Lett. **53**, 2053 (1988).

[23] T. A. Gant, M. Dutta, N. A. El-Masry, S. M. Bedair, and M. A. Stroscio, Phys. Rev. B **46**, 3834 (1992).

[24] K. Sinha, A. Mascarenhas, G. S. Horner, R. G. Alonso, K. A. Bertness, and J. M. Olson, Phys. Rev. B **48**, 17 591 (1993).

[25] A. Krost, N. Esser, H. Selber, J. Christen, W. Richter, D. Bimberg, L. C. Su, and G. B. Stringfellow, J. Cryst. Growth **145**, 171 (1994).

[26] K. Uchida, P. Y. Yu, N. Noto, Z. Lilienthal-Weber, and E. R. Weber, Philos. Mag. B **70**, 453 (1994).

[27] K. Sinha, A. Mascarenhas, G. S. Horner, K. A. Bertness, Sarah R. Kurtz, and J. M. Oslon, Phys. Rev. B **50**, 7509 (1994).

[28] F. Alsina, N. Mestres, J. Pascual, C. Geng, P. Ernst, and F. Scholz, Phys. Rev. B **53**, 12 994 (1996).

[29] N. Mestres, F. Alsina, J. Pascual, J. M. Bluet, J. Camassel, C. Geng, and F. Scholz, Phys. Rev. B **54**, 17 754 (1996).

[30] A. Hassine, J. Sapriel, P. Le Berrre, M. A. Di Forte-Poisson, F. Alexandre, and M. Quillec, Phys. Rev. B **54**, 2728 (1996).

[31] A. M. Mintairov and V. G. Melehin, Semicond. Sci. Technol. **11**, 904 (1996).

[32] H. M. Cheong, F. Alsina, A. Mascarenhas, J. F. Geisz, and J. M. Olson, Phys. Rev. B **56**, 1888 (1997).

[33] H. M. Cheong, A. Mascarenhas, P. Ernst, and C. Geng, Phys. Rev. B **56**, 1882 (1997).

[34] G. Lucovsky, M. H. Brodsky, M. F. Chen, R. J. Chicotka, and A. T. Ward, Phys. Rev. B **4**, 1945 (1971).

[35] R. Beserman, C. Hirliman, M. Balkanski, and J. Chavallier, Solid State Commun. **20**, 485 (1976).

[36] B. Ulrici and E. Jahne, Phys. Status Solidi B **86**, 517 (1978).

[37] E. Jahne, W. Pilz, M. Giehler, and L. Hildisch, Phys. Status Solidi B **91**, 155 (1979).

[38] I. F. Chang and S. S. Mitra, Phys. Rev. **172**, 924 (1968).

[39] B. Jusserand and S. Slempkes, Solid State Commun. **49**, 95 (1984).

[40] A. S. Barker, Jr. and A. J. Sievers, Rev. Mod. Phys. **47**, FS1 (1975).

[41] T. Kato, T. Matsumoto, and T. Ishida, Jpn. J. Appl. Phys., Part 1 **27**, 983 (1988).

[42] V. Ozoliņš and A. Zunger, Phys. Rev. B **63**, 087202 (2001).

[43] M. Kondow, S. Minagawa, and S. Satoh, Appl. Phys. Lett. **51**, 2001 (1987).

[44] H. Asahi, S. Emura, and S. Gonda, J. Appl. Phys. **65**, 5007 (1989).

[45] M. Kubo, M. Mannoh, Y. Takahashi, and M. Ogura, Appl. Phys. Lett. **52**, 715 (1988).

[46] D. P. Bour, J. R. Shealy, G. W. Wicks, and W. J. Schaff, Appl. Phys. Lett. **50**, 615 (1987).

[47] G. W. Wicks, D. P. Bour, J. R. Shealy, and J. T. Bradshaw, in

GaAs and Related Compounds 1986, edited by W. T. Lindley (IOP, Bristol, 1987).

[48] Z. C. Feng, E. Armour, I. Ferguson, R. A. Stall, T. Holden, L. Malikova, J. Z. Wan, F. H. Pollak, and M. Pavlosky, J. Appl. Phys. **85**, 3824 (1999).

[49] C. Kittel, *Introduction to Solid State Physics* (Wiley, New York, 1976).

[50] C. R. Pidgeon, in *Handbook on Semiconductors*, edited by M. Balkanski (North-Holland, Amsterdam, 1980), Vol. 2, pp. 223–328.

[51] G. E. Jellison, Thin Solid Films **313/314**, 33 (1998), and references therein.

[52] J. Humlíček, R. Henn, and M. Cardona, Appl. Phys. Lett. **69**, 2581 (1996).

[53] T. E. Tiwald, D. W. Thompson, and J. A. Woollam, J. Vac. Sci. Technol. B **16**, 312 (1998).

[54] Effects of multiple-component free-carrier plasmas can also be treated within this approximation: S. Zangooie, M. Schubert, D. Thompson, and J. A. Woollam, Appl. Phys. Lett. **78**, 937 (2001).

[55] T. E. Tiwald, J. A. Woollam, S. Zollner, J. Christiansen, R. B. Gregory, T. Wetteroth, S. R. Wilson, and A. R. Powell, Phys. Rev. B **60**, 11 464 (1999).

[56] J. Sik, M. Schubert, T. Hofmann, and V. Gottschalch, MRS Internet J. Nitride Semicond. Res. **5**, 3 (2000).

[57] G. Leibiger, V. Gottschalch, B. Rheinländer, J. Šik, and M. Schubert, J. Appl. Phys. **89**, 4927 (2001).

[58] J. Šik, M. Schubert, G. Leibiger, V. Gottschalch, and G. Wagner, J. Appl. Phys. **89**, 294 (2001).

[59] G. Leibiger, V. Gottschalch, and M. Schubert (unpublished).

[60] A. Kasic, M. Schubert, S. Einfeldt, D. Hommel, and T. E. Tiwald, Phys. Rev. B **62**, 7365 (2000).

[61] A. Kasic, M. Schubert, B. Kuhn, F. Scholz, S. Einfeldt, and D. Hommel, J. Appl. Phys. **89**, 3720 (2001).

[62] M. Schubert, A. Kasic, T. E. Tiwald, J. Off, B. Kuhn, and F. Scholz, MRS Internet J. Nitride Semicond. Res. **4**, 11 (1999); M. Schubert, A. Kasic, T. E. Tiwald, J. A. Woollam, V. Härle, and F. Scholz, *ibid.* **5**, W11 (2000).

[63] A. Kasic, M. Schubert, J. Off, and F. Scholz, Appl. Phys. Lett. **78**, 1526 (2001).

[64] R. Wirth, A. Moritz, C. Geng, F. Scholz, and A. Hangleiter, Phys. Rev. B **55**, 1730 (1997).

[65] P. Y. Yu and M. Cardona, *Fundamentals of Semiconductors* (Springer, Berlin, 1999).

[66] F. Gervais and B. Piriou, J. Phys. C **7**, 2374 (1974).

[67] F. Gervais and B. Piriou, Phys. Rev. B **11**, 3944 (1975).

[68] A. A. Kukharskii, Solid State Commun. **13**, 1761 (1973).

[69] J. Humlíček, R. Henn, and M. Cardona, Phys. Rev. B **61**, 14 554 (2000).

[70] M. Schubert, C. M. Herzinger, and T. E. Tiwald, Phys. Rev. B **62**, 7365 (2001).

[71] D. W. Berreman and F. C. Unterwald, Phys. Rev. **174**, 791 (1968).

[72] R. M. A. Azzam and N. M. Bashara, *Ellipsometry and Polarized Light* (North-Holland, Amsterdam, 1984).

[73] W. H. Press, B. P. Flannery, S. A. Teukolsky, and W. T. Vetterling, *Numerical Recipes: The Art of Scientific Computing* (Cambridge University Press, Cambridge, MA, 1988).

[74] Model parameters for GaAs were obtained from FIR-SE analysis of bare substrates and substrates with MOVPE-grown GaAs buffer layers. Values for ω_{TO}, ω_{LO}, $\gamma_{\mathrm{TO,LO}}$, and ϵ_{∞} were highly consistent within several samples and were not further varied here.

[75] M. Kondow, H. Kakibayashi, and S. Minagawa, Phys. Rev. B **40**, 1159 (1989).

[76] We do not distinguish between GaAs *A* and *B* planes; i.e., backscattering in $y'(x',z)\bar{y}'$ and $x'(y',z)\bar{x}'$ configuration is not distinguished.

[77] C. Ramkumar, K. P. Jain, and S. C. Abbi, Phys. Rev. B **53**, 13 672 (1996).

[78] M. Hass, *Optical Properties of III-V Compounds, Semiconductor and Semimetals* (Academic, New York, 1967), Vol. 3.

[79] O. K. Kim and W. G. Spitzer, J. Appl. Phys. **50**, 4362 (1979).

[80] M. H. Brodsky, G. Lucovsky, M. F. Chen, and T. S. Plaskett, Phys. Rev. B **2**, 3303 (1970).